Si(001):B gas-source molecular-beam epitaxy: Boron surface segregation and its effect on film growth kinetics

H. Kim, G. Glass, T. Spila, N. Taylor, S. Y. Park, J. R. Abelson, and J. E. Greene
Department of Materials Science, Coordinated Science Laboratory, and Materials Research Laboratory, University of Illinois, 1101 West Springfield, Urbana, Illinois 61801

(Received 17 March 1997; accepted for publication 12 May 1997)

B-doped Si(001) films, with concentrations C_B up to 1.7×10^{22} cm^{-3}, were grown by gas-source molecular-beam epitaxy from Si_2H_6 and B_2H_6 at $T_s=500-800$ °C. D_2 temperature-programed desorption (TPD) spectra were then used to determine B coverages θ_B as a function of C_B and T_s. In these measurements, as-deposited films were flash heated to desorb surface hydrogen, cooled, and exposed to atomic deuterium until saturation coverage. Strong B surface segregation was observed with surface-to-bulk B concentration ratios ranging up to 1200. TPD spectra exhibited β_2 and β_1 peaks associated with dideuteride and monodeuteride desorption as well as lower-temperature B-induced peaks β_2^* and β_1^*. Increasing θ_B increased the area under β_2^* and β_1^* at the expense of β_2 and β_1 and decreased the total D coverage θ_D. The TPD results were used to determine the B segregation enthalpy, -0.53 eV, and to explain and model the effects of high B coverages on Si(001) growth kinetics. Film deposition rates R increase by $\geqslant$50% with increasing $C_B\gtrsim1\times10^{19}$ cm^{-3} at $T_s\leqslant550$ °C, due primarily to increased H desorption rates from B-backbonded Si adatoms, and decrease by corresponding amounts at $T_s\geqslant600$ °C due to decreased adsorption site densities. At $T_s\geqslant700$ °C, high B coverages also induce {113} facetting. © *1997 American Institute of Physics.* [S0021-8979(97)03216-7]

I. INTRODUCTION

The use of disilane (Si_2H_6) rather than silane (SiH_4) for Si(001) gas-source molecular-beam epitaxy (GS-MBE) yields considerably higher deposition rates[1] due primarily to the fact that the Si–Si precursor bond is weaker than the Si–H bond.[2,3] We have previously employed a combination of reflection high-energy electron diffraction (RHEED), electron-energy-loss spectroscopy (EELS), and scanning tunneling microscopy (STM) to determine the mechanism and kinetics of Si GS-MBE from Si_2H_6.[2–7] Film deposition rates R are well described over wide ranges of incident Si_2H_6 fluxes and growth temperatures T_s (500–950 °C) using a model, with no fitting parameters, based upon dissociative Si_2H_6 chemisorption followed by a series of surface decomposition reactions with the rate-limiting step being first-order hydrogen desorption from Si monohydride.[3]

The incorporation probability of B from B_2H_6 in GS-MBE Si(001) has been shown to increase linearly with increasing B_2H_6/Si_2H_6 flux ratio and decrease exponentially with inverse film growth temperature.[8,9] B was incorporated into substitutional electrically active sites at concentrations C_B up to the highest value investigated, 2×10^{19} cm^{-3}, with no measurable effect on film growth rates R.[8] However, even higher B concentrations are of current interest in device fabrication for use as emitter layers in Si bipolar transistors,[10] base layers in $Si/Si_{1-x}Ge_x$ heterostructure bipolar transistors,[11] source and drain regions in metal–oxide–semiconductor transistors,[12] and as selectively grown epitaxial zero-level metallization.[12] Very highly doped Si:B/Si(001) heterostructures are also of interest for investigating strain relaxation mechanisms in layers under tension.[13]

Reported B equilibrium solid solubilities in Si range from 8×10^{20} cm^{-3} at 1400 °C (Ref. 14) to $\simeq1-1.5\times10^{20}$ cm^{-3} at 1000 °C (Refs. 15 and 16) and 2×10^{19} cm^{-3} at 700 °C.[16] B in Si(001) is known from combined ion channeling, cross-sectional transmission electron microscopy, and electrical measurements,[17] as well as more recent STM analyses,[18,19] to locate in the second atomic layer with a saturation coverage of 0.5 ML. The highest reported fully substitutional B concentration in GS-MBE Si(001) is 5×10^{20} cm^{-3}, obtained at $T_s=600$ °C.[20]

In this article, we present the results of experiments utilizing *in situ* D_2 temperature-programed desorption (TPD), reflection high-energy electron diffraction, and Auger electron spectroscopy (AES) to determine B surface coverages θ_B as a function of C_B ($5\times10^{16}-1.7\times10^{22}$ cm^{-3}) and T_s (500–800 °C) during GS-MBE Si(001):B growth. TPD spectra contain, in addition to β_1 and β_2 peaks due to monodeuteride $^DSi{=}Si^D$ and dideuteride $^DSi^D$ surface species, related lower-temperature B-induced β_1^* and β_2^* peaks associated with D-bonded Si* surface atoms with B backbonds. Fitting the four TPD peaks and comparing the results to our previous measurements on Si(001) wafers dosed with known B coverages[21] yields θ_B values for the films. For GS-MBE Si layers grown at $T_s=550$ °C, $\theta_B=0.10$ ML with $C_B=8.5\times10^{18}$ cm^{-3} and increases to saturation coverage, $\theta_{B,sat}=0.50$ ML, with C_B near 5×10^{20} cm^{-3}. At even higher B concentrations, an additional TPD peak is observed due to the presence of surface B–H bonds. Measured segregation ratios, $r_B=\theta_B/x_B$, where x_B is the bulk B concentration fraction, range from 50 to 1200 and the segregation enthalpy was determined to be -0.53 eV. Calculated $R(C_B,T_s)$ curves, based upon the TPD results, exhibit good agreement with deposition rate data.

 0021-8979/97/82(5)/2288/10/$10.00

II. EXPERIMENTAL PROCEDURE

All films were grown in a multichamber ultra-high-vacuum system, described in more detail in Ref. 8, evacuated using a combination of ion and turbomolecular pumps to provide a base pressure of $\simeq 5\times 10^{-11}$ Torr. The film growth chamber, equipped with a RHEED apparatus and a quadrupole mass spectrometer (QMS), is connected through the transfer chamber to an analytical station containing provisions for AES, EELS, low-energy electron diffraction, and TPD. The final system chamber contains a scanning tunneling microscope.

B-doped Si(001) films, 0.12–0.20 μm thick, were grown from Si_2H_6 and B_2H_6 molecular beams delivered to the substrate through individual directed tubular dosers located 3 cm from the substrate at an angle of 45°. The dosers are coupled to feedback-controlled constant-pressure reservoirs in which pressures are separately monitored using capacitance manometers whose signals are, in turn, used to control variable leak valves. Valve sequencing, pressures, gas flows, and substrate temperature are all computer controlled.

The Si(001) substrates were 1×3 cm^2 plates cleaved from 0.5 mm thick n-type (resistivity$=23$–$28\ \Omega$ cm, $n=1-2\times 10^{14}$ cm^{-3}) wafers. The initial cleaning consisted of degreasing by successive rinses in trichloroethane, acetone, propanol, and deionized water. The substrates were then subjected to four wet-chemical oxidation/etch cycles consisting of the following steps: 2 min in a 2:1:1 solution of H_2O:HCl:H_2O_2, rinse in fresh deionized water, and a 30 s etch in dilute (10%) HF. They were blown dry in dry ultra-high-purity N_2, exposed to a UV/ozone treatment, which consists of UV irradiation from a low-pressure Hg lamp (15 mW cm^{-2}) for 30 min in air to remove C-containing species,[22] and introduced into the deposition system through the transfer chamber where they were degassed at 600 °C for 4 h, cooled to 200 °C, and then rapidly heated at $\simeq 100$ deg s^{-1} to 1100 °C for 2 min to remove the oxide. The pressure never exceeded 5×10^{-9} Torr. RHEED patterns from substrates subjected to this procedure were 2×1 with sharp Kikuchi lines. No residual C or O was detected by AES.

The as-deposited B-doped Si(001) layers were transferred to the analytical chamber, heated to 700 °C for 10 s to desorb surface hydrogen, and then cooled to 200 °C. D_2 was delivered through a doser identical to those in the growth chamber and a hot W filament in the gas stream was used to crack the gas. All films were exposed to saturation D coverages. The TPD measurements were performed in the analytical chamber with the sample placed 2 mm from the 5 mm diam hole in the skimmer cone of a heavily differentially pumped Extrel QMS. Samples were heated at a linear rate, typically 2 °C s^{-1}, by direct current while the temperature was determined by a thermocouple calibrated using an optical pyrometer and desorption intensities were collected by computer. Deuterium was employed rather than hydrogen in order to suppress the background signal. Neither the flash heating for H desorption nor the TPD experiments themselves had any measurable effect on B segregation, as shown by the fact that B/Si AES ratios remain constant and successive TPD measurements yield identical results.

Deposited film thicknesses were measured using microstylus profilometry while B concentrations in as-deposited layers were determined using a Cameca IMS-5F secondary ion mass spectrometer (SIMS) operated with a 10 keV O_2^+ primary ion beam to detect ^{11}B. Quantification was carried out by comparison to B ion-implanted bulk Si standards yielding an experimental uncertainty of $\pm 10\%$. Other than intentionally introduced B, the films contained no detectable impurities.

High-resolution x-ray diffraction (HR-XRD) measurements were performed using a four-axis diffractometer with a Bartels four-crystal Ge monochromator and an Euler sample cradle with independent computer-controlled drive of all sample rotation angles. Cu $K\alpha$ radiation with an angular divergence <12 arc s and a wavelength spread of $\sim 2\times 10^{-5}$ was incident at an angle ω with respect to the sample surface. Reciprocal space maps were constructed by carrying out successive ω–2θ scans, centered at different values of ω, in the triple axis mode.[23]

Plan-view and cross-sectional transmission electron microscopy [(TEM) and (XTEM)] examinations were carried out in a Phillips CM120 microscope operated at 120 kV while high-resolution lattice images were obtained at 300 kV using a Hitachi H9000 microscope. Sample preparation for TEM and XTEM investigations followed the procedure described in Refs. 3 and 8.

III. RESULTS

A. Film growth

Doped Si(001) layers, 0.12–0.20 μm thick, were grown at $T_s=500$–800 °C with B concentrations C_B between 5×10^{16} and 1.7×10^{22} cm^{-3}. Typical zero-order Laue-zone RHEED patterns are shown in Fig. 1. Films grown at $T_s\leqslant 600$ °C with $C_B\leqslant 5\times 10^{19}$ cm^{-3} exhibited 2×1 patterns consisting of well-defined diffraction spots, rather than streaks, with sharp Kikuchi lines and essentially equi-intense fundamental and half-order reflections. The layer surfaces were thus atomically smooth with relatively large terraces. The RHEED pattern in Fig. 1(a) is from a film grown at $T_s=550$ °C with $C_B=8.5\times 10^{19}$ cm^{-3}. At higher B concentrations, the reflections become more streaky, as shown in Fig. 1(b) for a film with $C_B=2\times 10^{21}$ cm^{-3} ($T_s=550$ °C), the fundamental rods broaden, the half-order to fundamental rod intensity ratio decreases, and the amount of diffuse scattering increases; all are indicative of increased atomic-scale surface roughening.

RHEED patterns from films grown with $C_B\gtrsim 5\times 10^{19}$ cm^{-3} at $T_s=700$ °C and $\gtrsim 1\times 10^{19}$ cm^{-3} at 800 °C exhibit, in addition, indications of larger-scale surface roughening. An example is presented in Fig. 1(c) for a film with $C_B=3.5\times 10^{20}$ cm^{-3} ($T_s=800$ °C). Streaks, inclined with respect to the surface normal at angles of 25.2°, signifying the presence of {113} facets, are visible emanating from the tops and bottoms of both fundamental and half-order diffraction rods. ({113} facets have also been observed by XTEM in B-doped solid-source MBE Si films grown at $T_s=600$ °C with $C_B>1\times 10^{17}$ cm^{-3}.)[24] With still higher B concentrations, $C_B>10^{21}$ cm^{-3}, three-dimensional transmis-

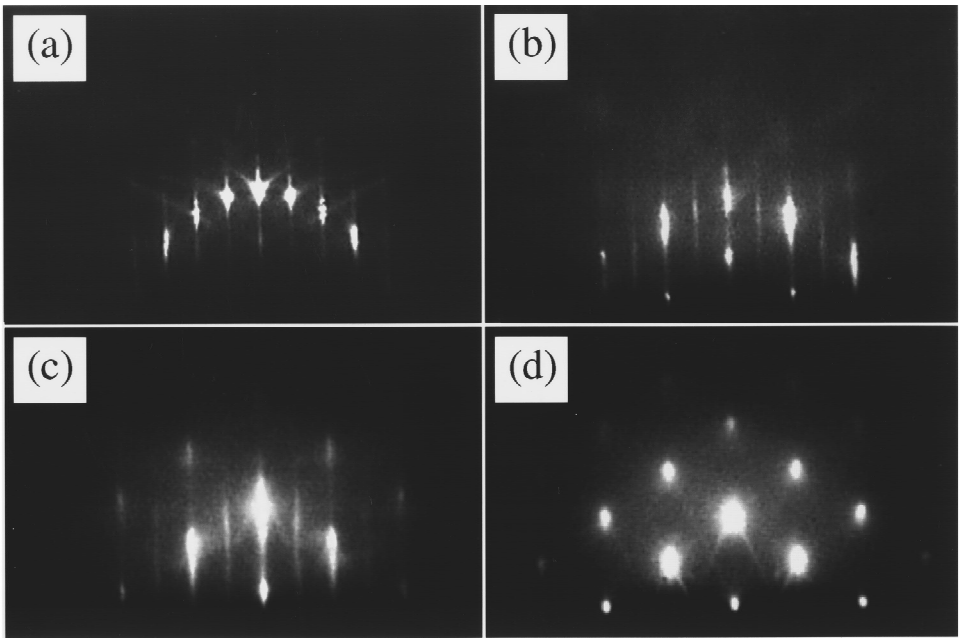

FIG. 1. RHEED patterns from GS-MBE Si(100):B films grown using Si_2H_6/B_2H_6 mixtures. Film growth temperatures T_s and B concentrations C_B are (a) $T_s=550$ °C, $C_B=8.5\times10^{18}$ cm^{-3}, (b) $T_s=550$ °C, $C_B=2\times10^{21}$ cm^{-3}, (c) $T_s=800$ °C, $C_B=3.5\times10^{20}$ cm^{-3}, and (d) $T_s=800$ °C, $C_B=3\times10^{21}$ cm^{-3}.

sion diffraction patterns were observed at $T_s\geqslant700$ °C, indicating an extremely rough surface. A typical result is shown in Fig. 1(d). TEM, XTEM, and HR-XRD reciprocal lattice mapping revealed no indication of dislocations or other extended defects in films with $C_B<5\times10^{20}$ cm^{-3}. The primary defects observed in films with higher B concentrations were {111} stacking faults.

Figure 2 shows undoped GS-MBE Si(001) growth rates as a function of temperature for a Si_2H_6 flux $J_{Si_2H_5}=2.2\times10^{16}$ cm^{-2} s^{-1}. The curve follows the general form expected for chemical vapor deposition in which R saturates at high temperatures in an impingement-flux-limited growth mode, while at low temperatures R decreases exponentially with $1/T_s$ indicative of surface-reaction-limited growth. For the Si_2H_6 flux used in the present experiments, temperature ranges for flux-limited and reaction-limited regimes are $T_s\gtrsim750$ °C and $T_s\lesssim625$ °C, respectively. The calculated curve in Fig. 2 shows that the undoped $R(T_s)$ data are well described by a model, developed in Ref. 3, based upon dissociative Si_2H_6 chemisorption followed by a series of surface decomposition reactions with the rate-limiting step being first-order hydrogen desorption from Si monohydride. The model contains no fitting parameters.

We find, in agreement with Ref. 8, that the use of B_2H_6 to provide B doping at concentrations up to $\simeq10^{19}$ cm^{-3} has no significant effect on GS-MBE Si growth rates. However, concurrent B doping during GS-MBE Si(001) with incident B_2H_6/Si_2H_6 flux ratios greater than $\simeq0.005$, corresponding to $C_B\gtrsim1.5\times10^{19}$ cm^{-3} at $T_s=550$ °C to 1×10^{20} at 800 °C, decreases the negative slope of $R(T_s)$ in the surface-reaction-limited regime. This has the effect of increasing R at low growth temperatures and decreasing it at higher temperatures, as shown in Fig. 2 for Si(001):B films grown with $C_B=1\times10^{20}$ cm^{-3}.

Figure 3 is a plot of R as a function C_B for 200 nm thick films grown at $T_s=550$, 600, 700 and 800 °C. The incident B_2H_6 flux was increased from 2.2×10^{12} to 6.6×10^{16} cm^{-2} s^{-1} ($J_{B_2H_6}/J_{Si_2H_6}=1\times10^{-4}-3$ with $J_{Si_2H_6}$ maintained at 2.2×10^{16} cm^{-2} s^{-1}). R remains constant with increasing B concentrations up to $\simeq10^{19}$ cm^{-3}, as noted above. At higher B doping levels, however, R increases by $\simeq50\%$ at $T_s=550$ °C (and by 60% at 500 °C, not shown). With $T_s\geqslant600$ °C, R decreases by comparable fractions, and

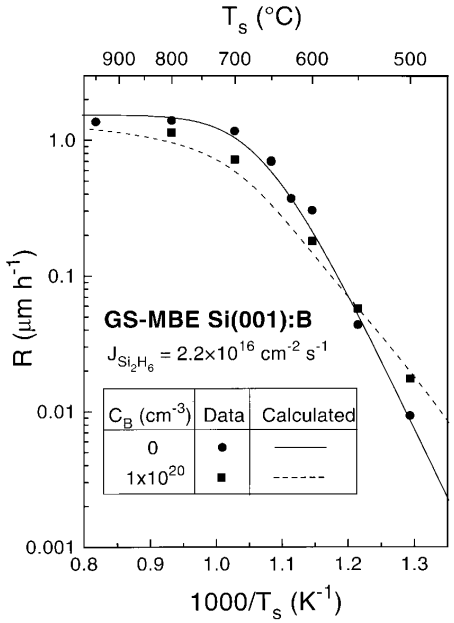

FIG. 2. Experimental (data points) and calculated (solid line, see Sec. IV) deposition rates R as a function of inverse temperature $1/T_s$ for GS-MBE Si(001) layers grown from Si_2H_6 and GS-MBE Si(001):B layers with $C_B=1\times10^{20}$ cm^{-3} grown from Si_2H_6/B_2H_6 mixtures.

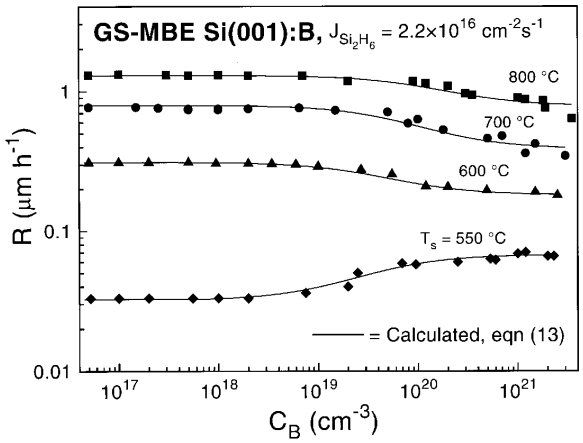

FIG. 3. Experimental (data points) and calculated (solid lines, see Sec. IV) GS-MBE Si(001):B deposition rates R as a function of the bulk B concentration C_B in layers grown from Si_2H_6/B_2H_6 mixtures with $J_{Si_2H_6}=2.2\times10^{16}\,cm^{-2}\,s^{-1}$.

the B concentration range over which the growth rate change is observed increases with increasing growth temperatures.

Typical SIMS profiles through a B modulation-doped sample are presented in Fig. 4. The Si(001) film was grown at $T_s=600\,°C$ with successive B-doped regions deposited for the same time and separated by 0.25 μm thick undoped buffer layers. $J_{Si_2H_6}$ was constant at $2.2\times10^{16}\,cm^{-2}\,s^{-1}$ while $J_{B_2H_6}$ was varied to provide C_B values from 1.7×10^{18} to $4.7\times10^{20}\,cm^{-3}$. In the more than 60 films grown for these experiments, there was no measurable B segregation in layers with $C_B\lesssim2\times10^{18}\,cm^{-3}$. SIMS profiles from these layers are essentially flat with the leading and trailing edges abrupt to within the experimental resolution, 8 nm per concentration decade. At higher B concentrations, however, significant B segregation is observed. The B incorporation probability during Si film growth is initially depressed, giving rise to SIMS profiles with ''missing'' B at the back side, as B accumulates at the surface until a steady-state ratio r_B of the surface-to-bulk B fractions is achieved. The value of r_B depends upon T_s, R, and $J_{B_2H_6}$. After turning off the B_2H_6 flux, the excess B at the surface acts as a reservoir to continue doping what was intended to be undoped buffer layers. A comparison of the widths of the profiles in Fig. 4 clearly shows, in agreement with the results in Fig. 3, that the Si deposition rate at 600 °C decreases with increasing C_B at high $J_{Si_2H_6}/J_{B_2H_6}$ ratios.

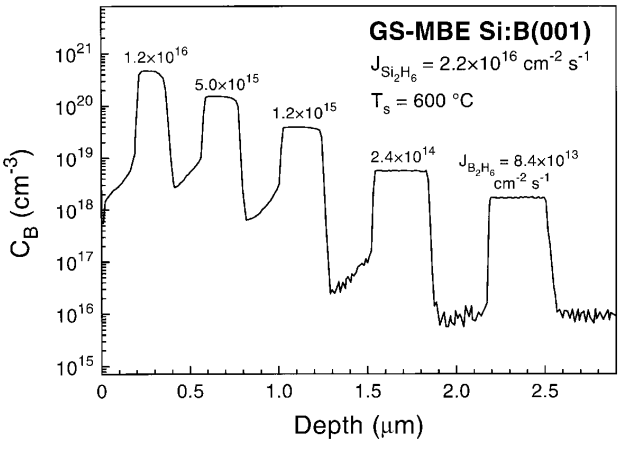

FIG. 4. SIMS depth profiles through a B modulation-doped Si(001):B film grown by GS-MBE from Si_2H_6 and B_2H_6 at $T_s=600\,°C$. The incident Si_2H_6 flux was $J_{Si_2H_6}=2.2\times10^{16}\,cm^{-2}\,s^{-1}$ while the B flux $J_{B_2H_6}$ was varied from 8.4×10^{13} to $1.2\times10^{16}\,cm^{-2}\,s^{-1}$. The deposition time for each layer was constant at 1 h.

B. TPD measurements

Typical D_2 TPD results from B-doped Si(001) films are reproduced in Figs. 5 and 6. Spectra from films with B concentrations less than $\simeq1\times10^{18}\,cm^{-3}$ [see, for example, Fig. 5(a)] are identical to those from clean Si(001) surfaces.[21] They consist of two peaks, labeled β_2 and β_1, due to desorption from the 1×1 dideuteride phase and the 2×1 monodeuteride phases, respectively. The peaks are centered at 405 and 515 °C. While β_2 desorption is second order, β_1 follows first-order kinetics, except at very low deuterium coverages $\theta_D<0.1$ ML,[25] due to π-bonding-induced pairing of dangling bonds on single dimers.[26]

At higher B concentrations, the TPD spectra change dramatically. The D_2 desorption onset temperature is reduced, the desorption features are broadened indicative of the presence of additional peaks, the high-temperature feature decreases in intensity while the low-temperature feature increases, and the total integrated area under the peaks decreases. Figures 5(b), 5(c), 5(d), and 5(e) are TPD spectra from $T_s=550\,°C$ Si(001) layers with $C_B=9\times10^{18}$, 4×10^{19}, 2.5×10^{20}, and $5.3\times10^{20}\,cm^{-3}$, respectively. The positions of the β_1 and β_2 peaks remain constant while two new peaks emerge, one at low temperature and one between the β_1 and β_2 peaks. The new low-temperature peak reduces the deuterium desorption onset temperature from 320 °C for Si(001) with $C_B\lesssim1\times10^{18}\,cm^{-3}$ to $\simeq250\,°C$ with $C_B=5.3\times10^{20}\,cm^{-3}$. Similar results were obtained with Si(001):B films grown at 600 °C except for an increase in the intensity ratio between the high-temperature and low-temperature features and in the total integrated area under the peaks. Thus, the 600 °C spectra are essentially identical to 550 °C spectra obtained from samples with lower B concentrations. An example TPD spectrum from a $T_s=600\,°C$ film with $C_B=4\times10^{19}\,cm^{-3}$ [compare with Fig. 5(c)] is shown in Fig. 5(f).

TPD spectra from layers with $C_B>1\times10^{19}\,cm^{-3}$ grown at higher temperatures follow the general trends observed in 600 °C samples, but become increasingly distorted as T_s is increased. Figure 6 shows TPD spectra from 800 °C films with $C_B=2\times10^{19}$, 1.2×10^{20}, 3.5×10^{20}, and $1.5\times10^{21}\,cm^{-3}$. The high-temperature TPD features are much wider than those observed at lower growth temperatures and overlap the low-temperature TPD features. In addition, at B concentrations $\gtrsim10^{21}\,cm^{-3}$, a new peak emerges near 300 °C and continues to increase in intensity. This peak strongly resembles the TPD feature in Fig. 7 obtained from an amorphous B film grown from B_2H_6 at 600 °C. The a-B layer was thick enough that no Si substrate signal was detected by AES.

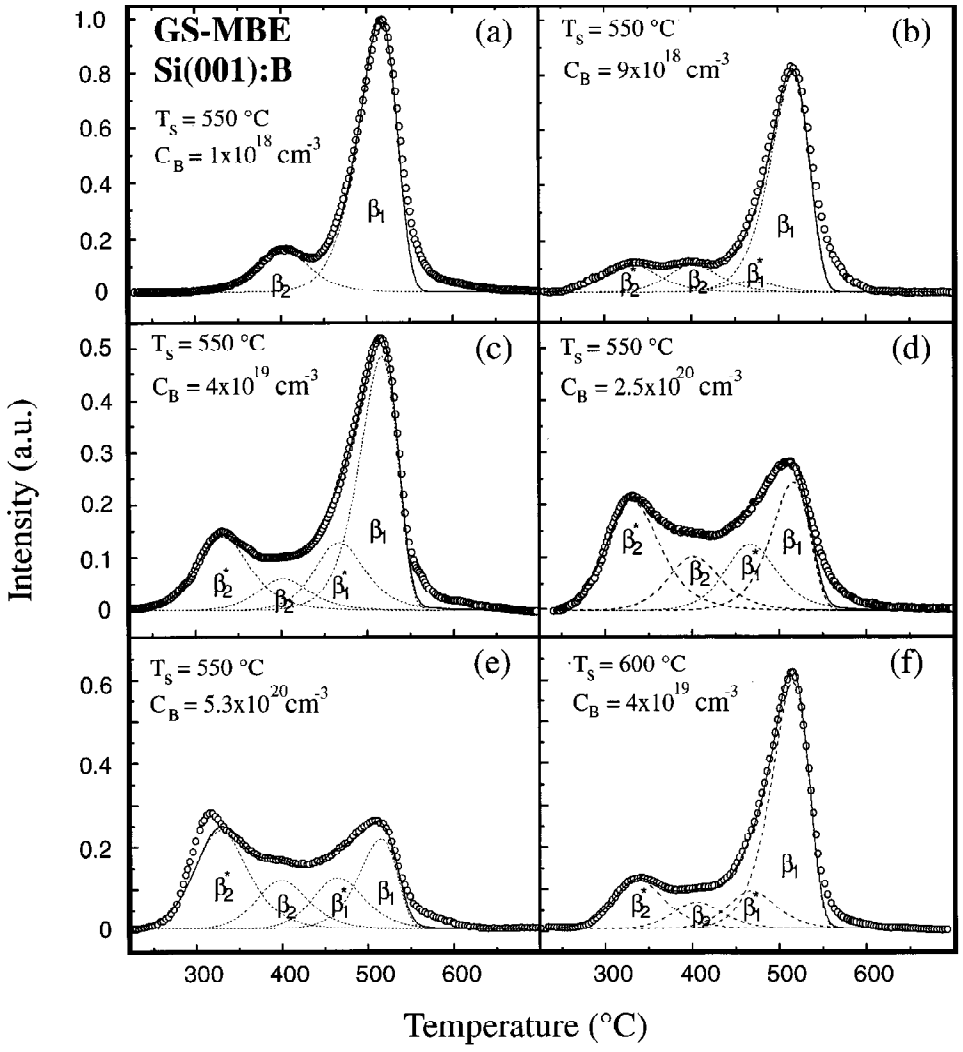

FIG. 5. D_2 TPD spectra from GS-MBE Si(001) films grown at $T_s = 550$ and 600 °C and doped with different B concentrations C_B. The same intensity scale is used in (a)–(f).

C. Calculated TPD spectra

All TPD spectra from B-doped epitaxial Si(001) layers were fitted using the standard Polanyi–Wigner analysis in which the desorption rate $d\theta_D/dT$ is expressed as[27]

$$\frac{d\theta_D}{dT} = -\left(\frac{\nu\theta_D^n}{\zeta}\right)\exp(-E_a/kT), \tag{1}$$

where ν is the attempt frequency, θ_D is the instantaneous D coverage, n is the order of the desorption reaction, ζ is the sample heating rate, E_a is the desorption activation energy, and k is Boltzmann's constant. At high pumping speeds,[28]

$$\ln\left(\frac{\theta_D(T)}{\theta_0}\right) = -\frac{\nu}{\zeta} I(T), \tag{2}$$

for first-order desorption and

$$\theta_D(T) = \frac{\theta_0}{1+(\nu/\zeta)\theta_0 I(T)}, \tag{3}$$

for second-order desorption. θ_0 in Eqs. (2) and (3) is the initial coverage and $I(T)$ is given by

$$I(T) = \frac{E_a}{R}\left|\frac{e^{-\epsilon}}{\epsilon^2}\sum_{n=1}^{\infty}\frac{(-1)^{n+1}n!}{\epsilon^{n-1}}\right|_{T_0}^{T}, \tag{4}$$

in which $\epsilon = E_a/kT$.

Spectra from samples with $C_B \lesssim 1\times10^{18}\,\mathrm{cm}^{-3}$, such as the results shown in Fig. 5(a), were fitted with E_a and ν equal to 1.88 eV and $1\times10^{13}\,\mathrm{s}^{-1}$ for β_2 and 2.52 eV and $1\times10^{15}\,\mathrm{s}^{-1}$ for β_1 as previously obtained for D_2 TPD from clean bulk Si(001) surfaces.[21] The agreement between measured and calculated spectra is very good except at high temperatures where the measured curves for both bulk Si(001) and the Si(001):B films are higher than the calculated curves due to the fact that β_1 desorption deviates from first-order kinetics at low deuterium (and hydrogen) coverages.[29]

All D_2 TPD spectra from films grown at $T_s = 500-600$ °C with C_B between 2×10^{18} and $3\times10^{20}\,\mathrm{cm}^{-3}$ were found to be well fit with four peaks: the initial β_2 and β_1 peaks together with two lower-temperature B-induced β_2^* and β_1^* peaks at 330 and 470 °C. Examples of fitted spectra are shown in Figs. 5(b)–5(d) for 550 °C and

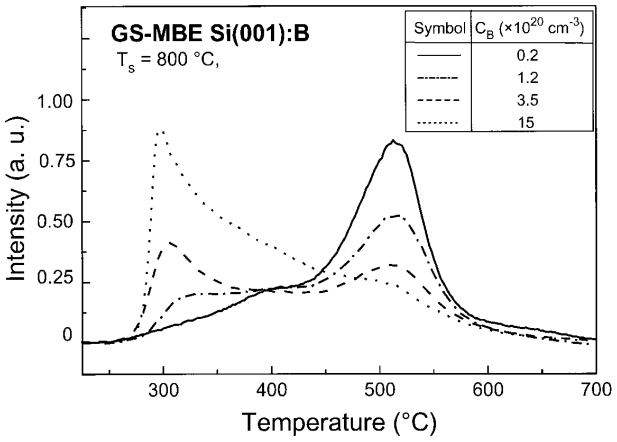

FIG. 6. D_2 TPD spectra from GS-MBE Si(001) films grown at $T_s = 800$ °C and doped with different B concentrations C_B. The intensity scale is the same as that used in Fig. 5.

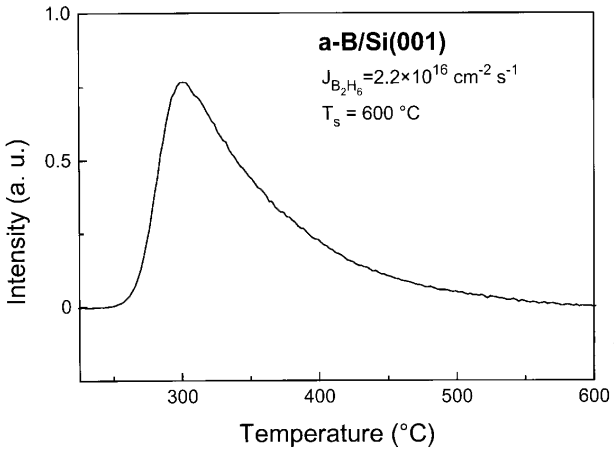

FIG. 7. D_2 TPD from an amorphous B layer deposited from B_2H_6 on Si(001) at $T_s = 600$ °C. The intensity scale is the same as that used in Figs. 5 and 6.

Fig. 5(f) for 600 °C samples. Best-fit values for E_a and ν are 1.56 eV and 1×10^{12} s^{-1} for β_2^* and 2.29 eV and 3×10^{14} s^{-1} for β_1^*, both peaks second order, again in agreement with our previous results for bulk Si(001) surfaces with known B coverages.[21]

TPD spectra from Si(001) films grown at $T_s \leqslant 600$ °C, but with $C_B > 5\times10^{20}$ cm^{-3}, were also well fit using the above parameters except at the low-temperature side where they exhibited an additional peak centered near 300 °C [see, for example, Figure 5(e)]. We believe that this new feature is an indication that the surface B coverage has exceeded the saturation value $\theta_{sat,B}$ of 0.5 ML and is due to desorption from surface B–D bonds consistent with the D_2 TPD spectra in Fig. 7 from an amorphous B film on Si.

At $T_s = 700$ and 800 °C with $C_B \gtrsim 5\times10^{19}$ and 1×10^{19} cm^{-3}, respectively, where RHEED patterns from Si(001) layers reveal the existence of 113 facets, the TPD spectra are more complex, as shown in Fig. 6. These results could not be fit with the same four peaks. The measured high-temperature features were much wider than β_1, and the β_2^* peak position did not match the low-temperature feature. Further attempts to fit these spectra would have to include desorption from 113 facets. The unreconstructed Si(113) surface consists of alternating single-atom-wide 001 and 111 steps in the [332] direction while the reconstructed Si(113) 3×2 surface is composed of dimers along [1$\bar{1}$0] on 001 steps and adatoms rebonded across 001 and 111 steps.[30] There are no reported hydrogen desorption results for Si(113).

D. B surface coverage

At all growth temperatures investigated, the total integrated TPD intensity decreased with increasing C_B. Examples were presented in Fig. 5 for $T_s = 550$ °C. These results show that the saturated deuterium coverage decreases with increasing B concentration in the films. This is due to the rapid decrease in β_1 while the integrated intensity under β_1^* increases slowly with increasing C_B. Ion channeling, cross-sectional transmission electron microscopy, and electrical measurements[17] together with STM analyses,[18,19] have shown that trivalent B atoms deposited on Si(001) move, primarily due to their smaller size,[21] to the second atomic layer and have a saturation coverage of 0.5 ML. Based upon STM results,[18,19] the primary B-induced Si(001) surface reconstruction at high coverages is a $c4\times4$ structural subunit containing four second-layer B atoms, two first-layer Si dimers having B backbonds, an unmodified first-layer Si dimer with Si backbonds, and a dimer vacancy. Thus, the decrease we observe in β_1 with increasing B concentration can be understood as being due to both B-induced dimer vacancies and a decrease in the dangling-bond density associated with Si dimers having Si backbonds, while the increase in β_1^* is due to the rising number density of Si dimers with B backbonds.

The overall decrease in θ_D with increasing C_B, and, hence, θ_B, is caused by two primary factors. The first is simply the fact that the Si dimer vacancy population increases in direct proportion to θ_B. This effect is exacerbated, however, by the partial deactivation of Si* (where Si* signifies a B-backbonded Si adatom) dangling bonds resulting from charge transfer from Si* adatoms to subsurface B, similar to the case for B/Si(111)$\sqrt{3}\times\sqrt{3}$ in which charge transfer was deduced from tunneling spectra.[31] The Si–B bond length, 2.0–2.1 Å,[32] is considerably shorter than Si–Si, 2.35 Å, and B has both a higher electronegativity than Si and an empty sp^3 orbital. Using measured β_1 and β_1^* integrated TPD peak intensities from bulk Si(001) wafers with known B coverages,[21] we find that approximately one dangling bond per Si* dimer is deactivated.

The deactivation of Si dangling bonds reduces the tendency for D atoms to pair up on single dimers and, thus, leads to the observed second-order β_1^* desorption kinetics. The lower activation energies measured for deuterium desorption from Si*–D and Si*–D_2 compared to Si–D and Si–D_2 result from the combination of Si*–B-backbond charge transfer and the additional strain in Si* dimers.

Based upon the ordered $c4\times4$ B subunit described above, the normalized coverage $\theta_{n,Si}$ of surface Si dimer atoms with Si backbonds decreases with increasing θ_B as

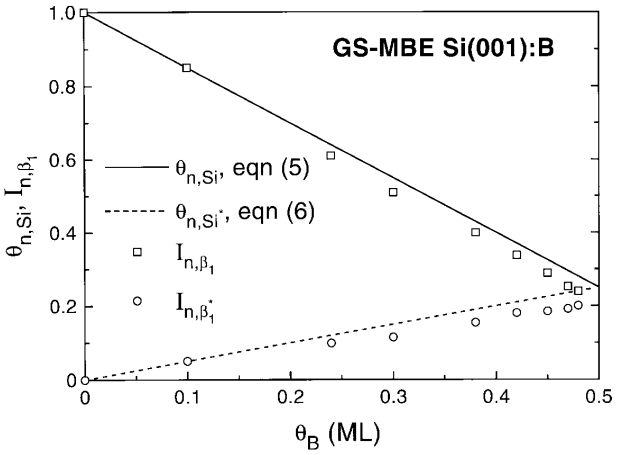

FIG. 8. Calculated normalized Si and Si* dimer atom coverages $\theta_{n,\mathrm{Si}}$ and $\theta_{n,\mathrm{Si}*}$ and measured normalized β_1 and $\beta_1^*D_2$ TPD peak intensities I_{n,β_1} and I_{n,β_1^*} as a function of steady-state B surface coverages θ_B on GS-MBE Si(001):B layers grown at $T_s=550$ °C.

$$\theta_{n,\mathrm{Si}}=1-1.5\theta_B, \tag{5}$$

and is represented by the solid line in Fig. 8. At the same time, the normalized coverage $\theta_{n,\mathrm{Si}*}$ associated with Si* dimer atoms increases from 0 to 0.50. However, since approximately half of these latter dangling bonds are deactivated, the effective value of $\theta_{n,\mathrm{Si}*}$ is

$$\theta_{n,\mathrm{Si}*}\simeq 0.5\theta_B, \tag{6}$$

as given by the dashed line in Fig. 8. The normalized integrated intensities under the β_1 and β_1^* TPD peaks I_{n,β_1} and I_{n,β_1^*} are also plotted in Fig. 8. B coverages, in this case, were obtained by setting the measured ratio $I_{n,\beta_1^*}/I_{n,\beta_1}=\theta_{n,\mathrm{Si}*}/\theta_{n,\mathrm{Si}}$. The results show that β_1 and β_1^* TPD intensities from Si:B films grown at constant T_s vary linearly with θ_B and exhibit good agreement with $\theta_{n,\mathrm{Si}}(\theta_B)$ and $\theta_{n,\mathrm{Si}*}(\theta_B)$, respectively. There is, however, a tendency for the calculated values of $\theta_{n,\mathrm{Si}}$ and $\theta_{n,\mathrm{Si}*}$ to slightly overestimate I_{n,β_1} and I_{n,β_1^*} as the B coverage approaches saturation. This is due primarily to the fact that the B-induced $c4\times4$ subunit also exists, although with lower probability, in other polymorphs,[19,20] and the overall fraction of deactivated Si* dangling bonds is actually a bit less than half.

Using the data in Fig. 8, the B surface coverage θ_B was plotted as a function of the bulk B concentration C_B, obtained from SIMS measurements. Figure 9(a) shows results for $T_s=550$ °C. Saturation B coverage, $\theta_B=0.5$ ML, is obtained at $C_B\simeq 5\times10^{20}\,\mathrm{cm}^{-3}$ with $T_s=550$ °C and $J_{\mathrm{Si_2H_6}}=2.2\times10^{16}\,\mathrm{cm}^{-3}$.

Estimates of second-layer B surface coverages in samples for which there was no TPD evidence for B in the first atomic layer (i.e., $\theta_B\leqslant\theta_{\mathrm{sat,B}}$) were obtained by AES, using the B KL_2L_2 (178 eV) and Si $L_{2,3}VV$ (92 eV) lines, for comparison to θ_B values obtained by TPD. AES sensitivity factors and electron escape lengths were taken from Ref. 33 and calibration was provided using a Si(111)$\sqrt{3}\times\sqrt{3}$ test sample which was known to have 0.33 ML of B in the third layer.[34] In analyzing the data, two limits were considered. In

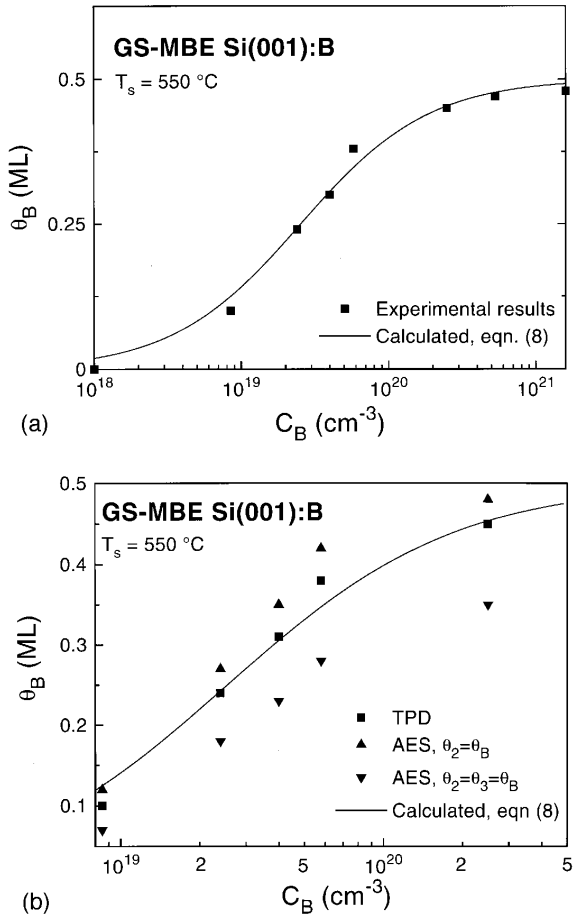

FIG. 9. (a) B surface coverages θ_B as a function of bulk B concentrations C_B in GS-MBE Si(001):B films grown from Si_2H_6/B_2H_6 mixtures at $T_s=550$ °C. (b) θ_B vs C_B data obtained from D_2 TPD measurements [replotted from (a)] compared with data obtained by AES assuming (i) all of the excess segregated B is in layer 2 and (ii) the segregated B is distributed equally in layers 2 and 3.

the first case, the B concentration in the bulk film is assumed to be constant and equal to C_B with excess segregated B located only in the second atomic layer. In case two, the excess B is evenly distributed in the second and third atomic layer. Both sets of results are shown in Fig. 9(b) and indicate, based upon the TPD data, that the majority of segregated B is in layer 2 with an increasingly smaller fraction of excess B in subsequent layers.

IV. DISCUSSION

Gibbsian surface segregation is described by the equation[35]

$$r_B=\frac{1-\theta_B}{1-x_B}\exp\left(\frac{-\Delta H_s}{kT_s}\right), \tag{7}$$

where r_B is the steady-state ratio of the surface coverage θ_B to the bulk B fraction x_B and ΔH_s is the segregation enthalpy. Expressing θ_B in terms of x_B, or C_B, and accounting for the fact that $\theta_{\mathrm{sat,B}}=0.5$ ML,[18–20] yields

$$\theta_B = \frac{0.5x_B \exp(-\Delta H_s/kT_s)}{1 - x_B + x_B \exp(-\Delta H_s/kT_s)} = \frac{0.5C_B \exp(-\Delta H_s/kT_s)}{n_{Si} - C_B\{1 - \exp(-\Delta H_s/kT_s)\}}, \quad (8)$$

where n_{Si} is the bulk Si atom density, 5×10^{22} cm^{-3}. Equation (8) is fitted to our θ_B versus C_B data in Fig. 9(a). Very good agreement is obtained using a segregation enthalpy $\Delta H_s = -0.53$ eV. To the best of our knowledge, this is the first result for GS-MBE Si:B, and is in reasonable agreement with reported ΔH_s values for B in solid-source MBE Si. Krüger and Osten[36] found $\Delta H_s = -0.44$ eV in MBE Si(001):B based upon fitting SIMS depth profiles while de Frésart *et al.*[37] obtained $\Delta H_s = -0.33$ eV in Si(111):B. In the latter case, the enthalpy was estimated using uncalibrated peak-to-peak AES measurements which, based upon our own AES results, tend to underestimate θ_B and, hence, $|\Delta H_s|$. Other comparable results for segregating species in solid-source MBE Si(001) include the group-IV alloying element Ge, $\Delta H_s = -0.28$ eV,[38] and oversize group-III and group-V dopants, In ($\Delta H_s = -0.85$ eV) (Ref. 39) and Sb ($\Delta H_s = -1.2$ eV).[35]

At elevated growth temperatures, dopant surface segregation approaches equilibrium values and r_B decreases with increasing temperature, while at low temperatures, where the segregation rate is of the order of or less than the film growth rate, segregation becomes kinetically limited and $r_B(T_s)$ decreases with decreasing temperature.[35] The transition T^* between kinetically limited and equilibrium dopant segregation decreases with decreasing film growth rate.[35] For solid-source MBE Si:B, T^* was found to range from 650 °C with $R = 1\ \mu$m h^{-1} to 600 °C at $R = 0.36\ \mu$m h^{-1}.[40] The present case is more complex since the steady-state hydrogen coverage $\theta_H(T_s, R)$ during GS-MBE also affects the B segregation rate. Nevertheless, using the solid-source MBE results as a guideline and accounting for the relatively low Si_2H_6 fluxes used in these experiments ($J_{Si_2H_6} = 2.2\times10^{16}$ cm^{-2} s^{-1} corresponding to $R = 0.03$–$0.06\ \mu$m h^{-1} at 550 °C and 0.3–0.2 μm h^{-1} at 600 °C), it is reasonable to expect that dopant segregation at $T_s \geqslant 550$ °C should be in the equilibrium regime. This is consistent with TPD spectra from films grown at 550 and 600 °C and having the same bulk B concentration [see, for example, Figs. 5(c) and 5(f) for which $C_B = 4\times10^{19}$ cm^{-3} and θ_B is 0.30 and 0.24, respectively] showing that r_B decreases with increasing T_s.

The film deposition rate during GS-MBE Si(001) from Si_2H_6 is given by[3]

$$R_{Si} = \frac{2S_{Si_2H_6}J_{Si_2H_6}}{n_{Si}}\,\theta_{db}^2, \quad (9)$$

where $S_{Si_2H_6}$ is the Si_2H_6 reactive sticking probability, 0.036,[3] and θ_{db} is the dangling-bond coverage. For Si:B film growth, we neglect the direct volume contribution of B to the film deposition rate since x_B is always less than 0.1 and for most cases of interest, less than 0.002. However, as discussed above, the presence of second-layer B atoms affects the total dangling-bond coverage, which can be expressed as

$$\theta_{db} = f\theta_{n,Si} + f^*\theta_{n,Si^*}, \quad (10)$$

in which f and f^* are the site fractions of Si and Si* which are unoccupied by H. From Eqs. (5), (6), and (8),

$$\theta_{n,Si} = \frac{n_{Si} - C_B\{1 - 0.25\exp(-\Delta H_s/kT_s)\}}{n_{Si} - C_B\{1 - \exp(-\Delta H_s/kT_s)\}} \simeq \frac{1 + 0.25(C_B/n_{Si})\exp(-\Delta H_s/kT_s)}{1 + (C_B/n_{Si})\exp(-\Delta H_s/kT_s)}, \quad (11)$$

and

$$\theta_{n,Si^*} = \frac{0.25C_B \exp(-\Delta H_s/kT_s)}{n_{Si} - C_B\{1 - \exp(-\Delta H_s/kT_s)\}} \simeq \frac{0.25(C_B/n_{Si})\exp(-\Delta H_s/kT_s)}{1 + (C_B/n_{Si})\exp(-\Delta H_s/kT_s)}. \quad (12)$$

Combining Eqs. (9)–(12), the growth rate of Si:B is given by

$$R_{Si} = \frac{2S_{Si_2H_6}J_{Si_2H_6}}{n_{Si}} \times \left(\frac{f + 0.25(f + f^*)(C_B/n_{Si})\exp(-\Delta H_s/kT_s)}{1 + (C_B/n_{Si})\exp(-\Delta H_s/kT_s)}\right)^2. \quad (13)$$

The term f in Eq. (13) can be expressed as a function of temperature during steady-state film growth,[3]

$$f = \frac{N_s k_d}{4S_{Si_2H_6}J_{Si_2H_6}}\left\{\left(1 + \frac{8S_{Si_2H_6}J_{Si_2N_6}}{N_s k_d}\right)^{1/2} - 1\right\}, \quad (14)$$

where $S_{Si_2H_6} = 0.36$ and $k_d(s^{-1}) = 7.9\times10^{11}\exp(-2.04\text{ eV}/kT_s)$. Equation (14) gives $f = 0.19$, 0.49, 0.87, and 0.99 with $T_s = 550$, 600, 700, and 800 °C. An initial estimate for f^* is obtained by measuring the fractional area, up to the film growth temperature T_s, under the corresponding β_1^* TPD peak. This yields $f^* = 0.67$, 0.89, 0.99, and 1 with $T_s = 550$, 600, 700, and 800 °C. These values are expected to be underestimates, primarily due to the rapid heating rate during TPD. Nevertheless, R versus C_B curves calculated from Eqs. (13) and (14) using these values exhibit good agreement at $T_s \leqslant 600$ °C, while at higher temperatures, the calculated curves, although they exhibit the correct shape, yield growth rates that are too low. Best fits were obtained using $f^* = 0.81$, 1.0, 1.4, and 2.2. These results, shown for 200 nm thick films in Fig. 3, agree very well with the experimental data. The necessity of using f^* values increasingly larger than unity to describe film growth kinetics at $T_s \geqslant 700$ °C is due to the presence of the {113} facets giving rise to higher surface site densities. In addition, the 113 surfaces can be expected to exhibit different Si_2H_6 reactive sticking probabilities and, as shown by the TPD spectra in Fig. 6, different B and Si*/Si site distributions.

Equations (13) and (14) were also used to calculate Si:B film growth rates as a function of temperature with C_B constant. $f^*(T_s)$ values were obtained from an equation similar to Eq. (14), but written (see Appendix) to account for the second-order desorption kinetics observed for β_1^*,

$$f^* = \left(1 + \sqrt{\frac{2S_{Si_2H_6}J_{Si_2H_6}}{N_s k_d^*}} \right)^{-1}, \tag{15}$$

where $k_d^* = \nu^* \exp(-E^*/kT_s)$ is the hydrogen desorption rate coefficient from surface Si* dimer atoms. Good agreement with $T_s = 550$ and 600 °C experimental results were obtained using $\nu^* = 5\times10^{11}$ s^{-1} and $E_a^* = 1.77$ eV, which yields f^* values similar to those obtained from direct measurements of β_1^* TPD fractional areas. An example of the agreement between calculated and measured $R(T_s)$ results is shown in Fig. 2 for films grown with $C_B = 1\times10^{20}$ cm^{-3}. The overall fit, even at high growth temperatures where 113 facetting requires the use of f^* values greater than 1, is reasonable.

The above analysis shows, as expected from the shape of the Si:B $R(T_s)$ curve in Fig. 2 and the TPD results, that the activation energy for hydrogen desorption from Si* surface atoms with B backbonds during steady-state film growth is significantly lower than from Si-backbonded surface atoms. That is, second-layer B atoms, whose concentration is enhanced by segregation, weaken surface Si–H bonds. Thus, in the lower-temperature $T_s \leqslant 550$ °C surface-reaction-limited growth regime where steady-state H coverages are high, R increases with increasing C_B, as shown in Figs. 2 and 3. At higher temperatures, corresponding to much lower steady-state θ_H values, the deactivation of Si dangling bonds increasingly becomes the dominant effect of second-layer B atoms and, thus, R decreases with increasing C_B. Note that in the flux-limited regime, where R remains essentially constant for pure Si growth, it continues to increase for Si:B. This is due to a decrease in $\theta_B(T_s)$ at high temperatures and the presence of the 113 facets.

V. CONCLUSIONS

We have shown that at high B doping concentrations in Si(001) films, ordered B subunits in the second layer weaken surface Si–H bonds while deactivating Si dimer dangling bonds during film growth. These effects are exacerbated by the strong tendency for B segregation giving rise to steady-state segregation ratios r_B up to 1200 at 550 °C. The segregation enthalpy ΔH_s was determined to be -0.53 eV. These results were used to model the effects of high B doping on Si:B GS-MBE growth kinetics. R increases with increasing $C_B \geqslant 2\times10^{19}$ cm^{-3} at $T_s \leqslant 550$ °C, where steady-state H coverages are high, due to B-enhanced H desorption rates. At $T_s \geqslant 600$ °C, corresponding to much lower steady-state θ_H values, R decreases due to B-induced deactivation of Si dangling bonds.

ACKNOWLEDGMENTS

The authors acknowledge the financial support of the Office of Naval Research through Contract Nos. NOOO 14-92-J-1649 and 14-96-0280, administered by Dr. Al Goodman and Dr. Larry Cooper, the Semiconductor Research Corporation, and the Department of Energy under Contract No. DEAC0276ER01198. The authors also thank Dr. H. H. Radamson and Mr. O. Gurdal for carrying out the HR-XRD and TEM analyses, respectively.

APPENDIX

The change in the surface dangling-bond density during GS-MBE of undoped Si(001) from Si_2H_6 is given by[3]

$$\frac{d\theta_{db}}{dt} = \frac{-2J_{Si_2H_6}S_{Si_2H_6}\theta_{db}^2}{N_s} + k_d(1-\theta_{db})^n, \tag{A1}$$

where Si_2H_6 adsorption is second order and hydrogen desorption is first order $(n=1)$. Thus, at steady state,

$$\theta_{db} = \frac{N_s k_d}{4S_{Si_2H_6}J_{Si_2H_6}} \left\{ \left(1 + \frac{8S_{Si_2H_6}J_{Si_2H_6}}{N_s k_d} \right)^{1/2} - 1 \right\}. \tag{A2}$$

In the case of Si(001):B, there are two types of surface Si dimer atoms, Si with Si backbonds and Si* with B backbonds. As in Eq. (10), the total dangling-bond coverage θ_{db} can be expressed as

$$\theta_{db} = f\theta_{n,Si} + f^*\theta_{n,Si^*}, \tag{A3}$$

in which $\theta_{n,Si}$ and $\theta_{n,Si*}$ are the normalized coverages of Si and Si*, while f and f^* are the corresponding dangling-bond site fractions. Thus, for the surface Si phase, f is given by Eq. (A2) above. However, the TPD results for β_1^* showed that desorption from B-backbonded Si is second order. The steady-state solution of Eq. (A1) with $n=2$ yields

$$f^* = \left(1 + \sqrt{\frac{2S_{Si_2H_6}J_{Si_2H_6}}{N_S k_d^*}} \right)^{-1}. \tag{A4}$$

[1] H. Hirayama, T. Tatsumi, and N. Aizaki, J. Cryst. Growth **95**, 476 (1989).
[2] D. Lubben, R. Tsu, T. R. Bramblett, and J. E. Greene, J. Vac. Sci. Technol. A **9**, 3003 (1991).
[3] T. R. Bramblett, Q. Lu, T. Karasawa, M.-A. Hasan, S. K. Jo, and J. E. Greene, J. Appl. Phys. **76**, 1884 (1994).
[4] Y. Suda, D. Lubben, T. Motooka, and J. E. Greene, J. Vac. Sci. Technol. B **7**, 1171 (1989); J. Vac. Sci. Technol. A **8**, 61 (1990).
[5] D.-S. Lin, E. S. Hirschorn, T.-C. Chiang, R. Tsu, D. Lubben, and J. E. Greene, Phys. Rev. B **45**, 3494 (1992).
[6] D.-S. Lin, T. Miller, T.-C. Chiang, R. Tsu, and J. E. Greene, Phys. Rev. B **48**, 11 846 (1993).
[7] G. Li, Y.-C. Chang, R. Tsu, and J. E. Greene, Surf. Sci. **330**, 20 (1995).
[8] Q. Lu, T. R. Bramblett, N.-E. Lee, M.-A. Hasan, T. Karasawa, and J. E. Greene, J. Appl. Phys. **77**, 3067 (1995).
[9] Q. Lu, T. R. Bramblett, M.-A. Hasan, J. E. Greene, J. Appl. Phys. **78**, 6027 (1995).
[10] T. Uchino, T. Shiba, T. Kikuchi, Y. Tamaki, A. Watanabe, and Y. Kiyota, IEEE Trans. Electron Devices **42**, 406 (1995).
[11] Z. Matutinovickrstelj, V. Venkataraman, E. J. Prinz, J. C. Sturm, C. W. Magee, IEEE Trans. Electron Devices **43**, 457 (1996).
[12] Y. Kinoshita, K. Imai, H. Yoshida, H. Suzuki, T. Tatsumi, and T. Yamazaki, Proceedings of the International Electron Device Meeting, San Francisco, December, 1994 (IEEE, New York, 1994), p. 441; Y. Kiyota, T. Nakamura, S. Suzuki, and T. Inada, IEEE Trans. Electron Devices **79C**, 554 (1996).
[13] B. Tillack, P. Zaumseil, G. Morgenstern, D. Krüger, B. Dietrich, and G. Ritter, J. Cryst. Growth **157**, 181 (1995).
[14] S. M. Sze, *Physics of Semiconductor Devices*, 2nd ed. (Wiley, New York, 1981), p. 69.
[15] F. N. Schwettman, J. Appl. Phys. **45**, 1918 (1974).
[16] G. L. Vick and K. M. Whittle, J. Electrochem. Soc. **119**, 1142 (1969).
[17] R. L. Headrick, B. E. Weir, A. F. Levi, D. J. Eaglesham, and L. C. Feldman, Appl. Phys. Lett. **57**, 2779 (1990).
[18] Y. Wang, and R. J. Hamers, Appl. Phys. Lett. **56**, 2057 (1995); J. Vac. Sci. Technol. A **13**, 1431 (1995).
[19] Y. Wang, R. J. Hamers, and E. Kaxiras, Phys. Rev. Lett. **74**, 403 (1995).
[20] G. Glass, H. Kim, M. R. Sardela, Q. Lu, J. A. Abelson, and J. E. Greene, Surf. Sci. Lett. (submitted).

[21] H. Kim, G. Glass, S. Y. Park, T. Spila, N. Taylor, J. R. Abelson, and J. E. Greene, Appl. Phys. Lett. **69**, 3869 (1996).
[22] X.-J. Zhang, G. Xue, A. Agarwal, R. Tsu, M.-A. Hasan, J. E. Greene, and A. Rockett, J. Vac. Sci. Technol. A **11**, 2553 (1993).
[23] Q. Lu, M. R. Sardela, Jr., T. R. Bramblett, and J. E. Greene, J. Appl. Phys. **80**, 4458 (1996).
[24] X. Lu, Z. Jiang, H. Zhu, X. Zhang, and X. Wang, Appl. Phys. Lett. **68**, 3278 (1996).
[25] U. Höfer, L. Li, and T. F. Heinz, Phys. Rev. B **45**, 9485 (1992).
[26] J. J. Boland, J. Vac. Sci. Technol. A **10**, 2458 (1992).
[27] P. A. Redhead, Vacuum **12**, 203 (1962).
[28] F. M. Lord, J. S. Kittelberger, Surf. Sci. **43**, 173 (1974).
[29] G. Boishin and L. Surnev, Surf. Sci. **345**, 64 (1966).
[30] J. Knall, J. B. Pethica, J. D. Todd, and J. H. Wilson, Phys. Rev. Lett. **66**, 1733 (1991).
[31] Ph. Avouris, I.-W. Lyo, F. Bozso, and E. Kaxiras, J. Vac. Sci. Technol. A **8**, 3405 (1990).
[32] B. E. Weir, R. L. Headrick, Q. Shen, L. C. Feldman, M. S. Hybertson, M. Needels, M. Schluter, and T. R. Hart, Phys. Rev. B **46**, 12 861 (1992).
[33] C. C. Chang, Surf. Sci. **48**, 9 (1975).
[34] P. J. Chen, M. L. Colaianni, and J. T. Yates, Jr., J. Appl. Phys. **72**, 3155 (1992).
[35] S. A. Barnett and J. E. Greene, Surf. Sci. **151**, 67 (1985).
[36] D. Krüger and H. J. Osten, Thin Solid Films **258**, 137 (1995).
[37] E. de Frésart, K. L. Wang, and S. S. Rhee, Appl. Phys. Lett. **53**, 48 (1988).
[38] S. Fukatsu, K. Fujita, H. Yaguchi, Y. Shiraki, and R. Ito, Appl. Phys. Lett. **59**, 2103 (1991).
[39] A. Rockett, S. A. Barnett, J. E. Greene, J. Knall, and J. E. Sundgren, J. Vac. Sci. Technol. A **3**, 855 (1985).
[40] C. P. Parry, R. A. Kubiak, S. M. Newstead, T. E. Whall, and E. H. C. Parker, Mater. Res. Soc. Symp. Proc. **220**, 79 (1991); C. P. Parry, R. A. Kubiak, S. M. Newstead, E. H. C. Parker, and T. E. Whall, *ibid.* **220**, 103 (1991).